JSR Publications

Available Online

J. Sci. Res. **16** (3), 745-756 (2024)

JOURNAL OF SCIENTIFIC RESEARCH

www.banglajol.info/index.php/JSR

Effect of Eu^{3+} Ion on the Optical and Photoluminescence Properties of Chemically Synthesized CaF_2 Nanoparticles

N. S. Devi[1], M. R. Shiekh[2], L. R. Singh[3*], A. N. Singh[4]

[1]Department of Physics, Manipur University, Canchipur, Manipur, India

[2]Moirang College, Moirang, Manipur, India

[3]Department of Physics, D.M. College of Sciences, Imphal, Dhanamanjuri University, Manipur, India

[4]D.M. College of Commerce, Imphal, Dhanamanjuri University, Manipur, India

Received 19 March 2024, accepted in final revised form 8 June 2024

Abstract

Pure CaF_2 and CaF_2:Eu^{3+} nanoparticles were synthesized by solution combustion method. The structural characterization of the samples was done by XRD (X-ray diffraction). The average crystallite size for CaF_2 and CaF_2:Eu^{3+} nanoparticles was found to be 17.11 nm and 32.53 nm respectively. The surface morphology was studied by FESEM (Scanning Electron Microscope) and formation of nanospheroids was observed. The EDAX analysis confirmed the purity of the synthesized samples. The band gap energy of the samples was estimated by UV-Visible Spectroscopy. CaF_2 was found as direct band gap material of 3.87 eV and CaF_2:Eu^{3+} as indirect band gap material of 4.99 eV respectively. The photoluminescence excitation peak for CaF_2 was observed around 387 nm and the emission peak was observed around 420 nm. The photoluminescence excitation peaks for CaF_2:Eu^{3+} were observed around 299 nm, 317 nm, 361 nm and 394 nm respectively and the emission peaks were observed around 591 nm and 616 nm respectively.

Keywords: Band gap; Combustion; Nanoparticles; Photoluminescence.

doi: https://dx.doi.org/10.3329/jsr.v16i3.72000 J. Sci. Res. **16** (3), 745-756 (2024)

1. Introduction

During the last two decades, many comprehensive discoveries in the field of nanomaterials and their applications have been achieved. Among them, nanoparticles of lanthanide (III)-doped alkali halides are becoming the potential candidates for several applications in electrical and optical devices. Further, among the different halide compounds, fluoride compounds are well-known host materials for lanthanide (III)-doped nanocrystals because of its high transparency, low phonon energy and low refractivity [1-4]. It may be noted from literature review that many researchers worked on Eu^{3+} ion doped CaF_2 nanoparticles. Recently, in the year 2021, Fang *et al*. studied the enhancement in luminescence properties

* *Corresponding author*: laishramraghumani204@gmail.com

of Eu^{3+} doped CaF_2 nanoparticles synthesized by Bridgman-Stockbarge method [5]. The structural and photoluminescence properties of Eu^{3+} doped CaF_2 nanocubes synthesized by direct precipitation route have been studied by Cantelar *et al*. [6]. Malviya *et al.* also reported the structural and optical properties of Eu^{3+} doped CaF_2:Eu^{3+} nanoparticles synthesised by ultrasound assisted method in 2019 [7]. Since CaF_2 possesses high stability and non-hygroscopic behaviour, it can be considered as an important class of fluorides and has been used as a host nanomaterial. As a result, Eu^{3+} ion doped CaF_2 nanoparticles have been examined in fundamental as well as applied studies for different applications [8-13]. For applications in optical and optoelectronic devices, band gap energy is a key factor in evaluating their performance. Anghel *et al*. also reported the dedicated optoelectronic properties of rare earth ions (Eu^{3+}) doped CaF_2 nano crystals [14]. Recently, many researchers have been attracted towards the light emitting phosphors in the field of luminescence also. Among various lanthanide ions, Eu^{3+} ion can be efficiently used as red luminescent phosphor because of its emissions in the visible region of spectrum corresponding to transition, $^5D_0 \rightarrow ^7F_J$ (J = 0 – 4) and such transitions originate from the inner 4f electrons which are shielded from their outer filled 5s and 5p shells. As the Eu^{3+} ion has long luminescence lifetimes, it can exhibit low absorption coefficient also. Wang and Lieu also reported that there are many criteria for choosing the host lattice which matches to dopant ions [15]. It was found that the fluorides can be used as the suitable host lattice for designing of luminescent phosphors.

As reported in literature, CaF_2 nanoparticles are generally synthesized by the liquid-phase methods. The liquid-phase methods include co-precipitation [16], hydrothermal (high temperature hydrolysis) [17], Sol-gel and (colloidal chemistry) [18] and radiation chemical synthesis [19]. But, in the present research work, we follow the solution combustion method to synthesize Eu^{3+} doped CaF_2 nanoparticles because of its advantages like high purity of resulting nanoparticles, short duration for synthesis, non-toxic or non-hazardous reagents are used and less expensive. After structural characterization, the optical properties of synthesized CaF_2 and Eu^{3+} ion doped CaF_2 nanoparticles will be studied for estimation of its band gap energy and we will investigate whether there is transformation in nature of band gap i.e from direct band gap to indirect band gap on doping of Eu^{3+} ion. The photoluminescence properties of the synthesized samples will be studied for determination of its behaviour of luminescent phosphor towards the fabrication of different lasers producing different colours of light.

2. Experimental Section

2.1. *Materials*

Calcium nitrate, $Ca(NO_3)_2$ (99.9 %) purchased from Sigma Aldrich, product of China was used as the source of calcium ion. Ammonium fluoride, NH_4F (99.9 %) purchased from Sigma Aldrich, product of Germany was used as the source of fluoride ion. Europium nitrate, $Eu(NO_3)_3$ (99.9 %) purchased from Sigma Aldrich, product of USA was used as the

source of dopant. Urea, $CO(NH_2)_2$ (> 99 %) purchased from Merck ACS , Mumbai, India was used as the fuel.

2.2. *Method of synthesis*

Pure and Eu^{3+} doped CaF_2 Nanoparticles were synthesized by solution combustion method. For synthesis of pure CaF_2, a clear solution of $Ca(NO_3)_2$ was prepared by dissolving 0.01 mol of $Ca(NO_3)_2$ in 20 mL of distilled water. Similarly, a clear solution of NH_4F was also prepared by dissolving 0.01 mol of NH_4F in 20 mL of distilled water separately. Then, the prepared solutions were mixed together and 1 mol% of Urea, $CO(NH_2)_2$ which is used as fuel, was added to the same. The resultant mixture was stirred using a magnetic stirrer maintaining the temperature at 30 °C until a gelatinous composition is observed. The sample was then placed in the muffle furnace at 500 °C for combustion and combustion takes place spontaneously within 10-18 sec thereby forming CaF_2 Nanoparticles. The powder was again annealed at 400 °C for 1.30 h in order to increase crystal growth.

For synthesis of Eu^{3+} doped CaF_2 nanoparticles i.e. CaF_2:Eu^3, 0.1 mol%. of $Eu(NO_3)_3$ was added to the $Ca(NO_3)_2$ solution and the same was stirred for 30 min. The mixture solution was mixed with precursor of NH_4F and 1 mol% of Urea, $CO(NH_2)_2$ following the same procedure for production of CaF_2:Eu^{3+} nanoparticles.

3. Results and Discussion

3.1. *Structural study*

The structural characterization was done by an X-ray diffractometer (Bruker D8 Advance) in the 2θ range (20°–80°) using CuKα radiation of wavelength λ = 1.5406A°. The XRD patterns of CaF_2 and CaF_2:Eu^{3+} nanoparticles are shown in Fig. 1. The formation of CaF_2 having simple cubic crystal structure is confirmed by the standard reference JCPDS Card No. 00-004-0864 with space group : Fm-3 m. The five peaks corresponding to crystal planes (111), (220), (311), (400) and (331) are observed in the XRD patterns. However, the extremely low intensity peaks corresponding to crystal planes (400) and (331) can be discarded as the atomic density is very low for analysis. The narrow and sharp peaks corresponding to crystal planes (111) and (220) indicate that the synthesized materials have good crystallinity. Further, it is also confirmed that no other diffraction peaks of other substances are detected. This implies that the introduction of Eu^{3+}ions on CaF_2 does not change the crystal structure of the product. No impurity phase can be detected. Thus, it reveals that we have successfully prepared CaF_2 and CaF_2:Eu^{3+}nanoparticles. The structural parameters of CaF_2 and CaF_2:Eu^{3+} nanoparticles are shown in Table 1. The inter planar spacing (d spacing) is calculated by using Bragg's equation,

$$n\lambda = 2d\sin\theta \quad (1)$$

where λ = 1.5406 A^0, θ = diffraction angle in degrees, n = 1 (Order of diffraction), d = inter planar spacing or d spacing (in A°). The d spacing values are comparable with the

standard values as shown in Table 1. It is observed that the d-spacing for each crystal plane is found to increase on doping of Eu^{3+} ion as shown in Table 1. It is because of the fact that the ionic radius of dopant ion i.e Eu^{3+} ion (0.106 nm) is larger than that of host material i.e. Ca^{2+} ion (0.099 nm).

The lattice constants for cubic structure is calculated by using the relation

$$a = d(h^2 + k^2 + l^2)^{1/2} \quad (2)$$

The value of lattice constants as shown in Table 1. This value is also in good agreement with literature value, a = 5.435 Aº [20]. It is also observed that the value of lattice constant i.e. lattice size slightly increase on doping of Eu^{3+} for each plane as shown in Table 1. This leads to produce the slight shift of diffraction peak of CaF_2:Eu^{3+} before the diffraction peak of CaF_2 (host material) i.e. shifting of peaks takes place towards smaller value of 2θ in XRD pattern as shown in Fig. 1. Jianfu Pan et al. also reported the similar shifting of diffraction peaks and the increase in lattice constant of CaF_2 nanoparticles on doping of Eu^{3+} ions due to different ionic radius and charge of Eu^{3+} ion from Ca^{2+} ion [21].

The strain is calculated by using the tangent formula,

$$\varepsilon = \frac{\beta}{4\tan\theta} \quad (3)$$

where β = FWHM in radian, θ = diffraction angle in degrees. The strain value of a crystal shows the alignment of a crystal that was produced. It is observed that the strain values for each plane are found to decrease on doping of Eu^{3+} ion. It is because of the fact that smaller peak broadening is produced in CaF_2:Eu^{3+} crystals as compared to that in pure CaF_2 crystals, which is also observed in XRD pattern as shown in figure 1.

The crystallite size of CaF_2 and CaF_2:Eu^{3+} crystals is calculated by using Scherrer's formula,

$$D = \frac{k\lambda}{\beta\cos\theta} \quad (4)$$

where *K* is a constant (= 0.94), β is the full width at half maximum (FWHM) in radian of the diffraction peak corresponding to a particular crystal plane [22]. The average crystallite sizes for CaF_2 and CaF_2:Eu^{3+} are found to be 17.11 nm and 32.53 nm respectively. This indicates that the crystallite size of CaF_2 increases on doping of Eu^{3+}. This is due to the fact that when Ca^{2+} ions are substituted by a rare earth ion (Eu^{3+}), the charge compensating F^- ions enter the fluorite structure in interstitial cubic sites and experience repulsion which leads to increase of the lattice parameters. The similar results for RE element doped CaF_2 nanoparticles have been reported by Reddy and Pandurangappa [23].

The dislocation density is calculated by using the formula

$$\rho = \frac{1}{D^2} \quad (5)$$

and it states the number of dislocation lines per unit volume of crystal i.e. the size of the crystal defects possessed by a crystal. In other words, the dislocation density value will illustrate the degree of crystallinity of the nanoparticles profile. The small dislocation density value indicates high degree of crystallinity. The dislocation density value of pure CaF_2 crystal is found to be larger than that of CaF_2:Eu^{3+} crystal as shown in Table 1. This indicates that the pure CaF_2:Eu^{3+} crystal possesses high degree of crystallinity as compared to CaF_2 crystal which can be correlated with XRD pattern as shown in Fig. 1.

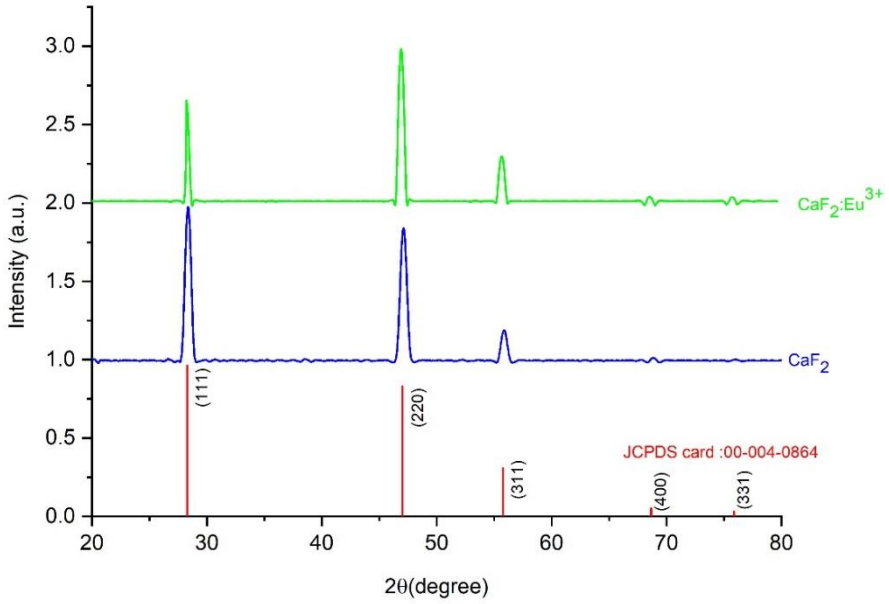

Fig. 1. XRD pattern of CaF_2 and $CaF_2:Eu^{3+}$ nanoparticles.

Table 1. Sturctural parameters of CaF_2 and $CaF_2:Eu^{3+}$ nanoparticles.

Sample	2θ (degree)	(hkl)	d-spacing calculated value (A^0)	d-spacing standard value (A^0)	a (A^0) calculated value	Strain, ε	Crystallite size, D (nm)	Av. value of D (nm)	Dislocation density, δ $(nm)^{-2}$
CaF_2	28.363	(111)	3.150	3.153	5.455	9.11×10^{-3}	16.20	17.11	0.00341
	47.050	(220)	1.930	1.931	5.458	4.81×10^{-3}	18.85		
	55.819	(311)	1.645	1.647	5.455	4.74×10^{-3}	16.30		
$CaF_2:Eu^{3+}$	28.184	(111)	3.164	3.153	5.480	4.91×10^{-3}	30.26	32.53	0.000945
	46.865	(220)	1.937	1.931	5.478	2.76×10^{-3}	32.95		
	55.684	(311)	1.649	1.647	5.469	2.25×10^{-3}	34.40		

3.2. *EDAX analysis*

The elemental composition of the synthesized samples are analysed by EDAX. The spectra of the pure CaF_2 and $CaF_2:Eu^{3+}$ nanoparticles obtained by EDAX analysis are shown in Figs. 2(a,b) respectively. The EDAX analysis indicates that the as prepared sample consists of Calcium, Fluorine and Europium.

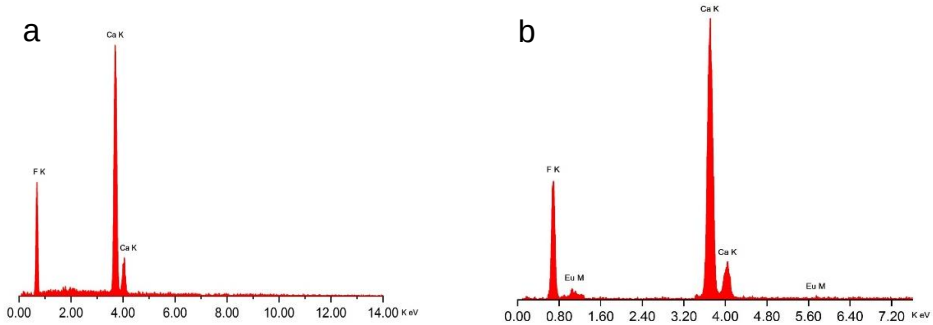

Fig. 2. EDAX spectra of (a) pure CaF_2 (b) CaF_2:Eu^{3+} nanoparticles.

3.3. *Morphological study*

Figs. 3(a,b) show FESEM images of pure CaF_2 and CaF_2:Eu^{3+} nanoparticles synthesized by solution combustion method respectively. The FESEM images reveal the formation of rough spherical structures which may be called as nanospheroids. The size (diameter) of as synthesized nanospheroids is estimated by using image j software. The compactness or agglomeration of nanospheroids increases on doping of Eu^{3+}ions in host lattice of Ca^{2+}ions. The histograms i.e. frequency of occurrence versus diameter of the CaF_2 and CaF_2:Eu^{3+} nanospheroids are shown in Figs. 4(a,b) respectively. From the histogram, the average diameter of the nanospheroids is found to be 66 nm for pure CaF_2 and 113.52 nm for CaF_2:Eu^{3+} nanoparticles. It has been observed that the average diameter of Eu^{3+} doped CaF_2 nanospheroids is larger than that of pure CaF_2 nanospheroids which is consistent with XRD results.

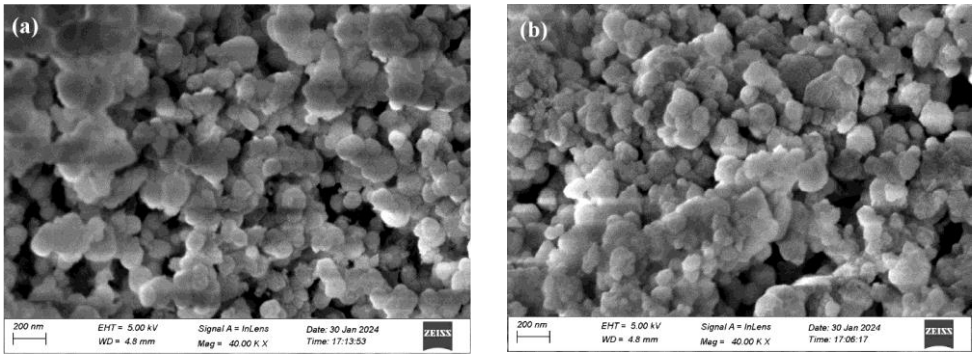

Fig. 3. FESEM images of (a) pure CaF_2 (b) CaF_2:Eu^{3+} nanoparticles.

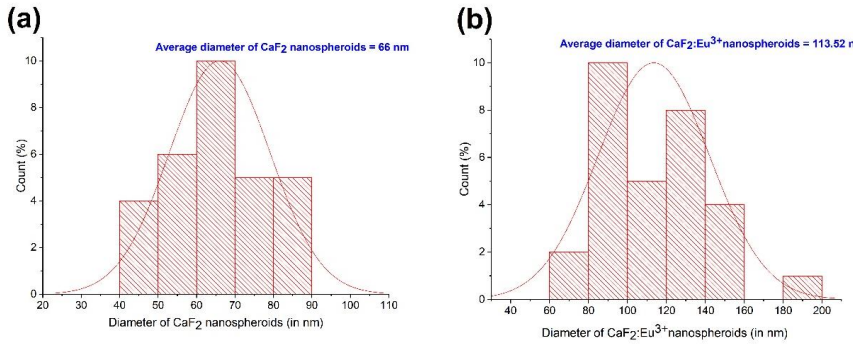

Fig. 4. Histograms of (a) pure CaF_2 (b) CaF_2:Eu^{3+} nanoparticles.

3.4. *Optical study*

The optical properties of pure CaF_2 and Eu^{3+} doped CaF_2 i.e. CaF_2:Eu^{3+} nanoparticles are studied with the help of UV-Visible Spectroscopy. The values the energy band gap of pure as well as doped samples are calculated from Tauc relation [24].

$$(\alpha h\nu)^{\gamma} = A(h\nu - E_g) \quad (6)$$

where α is absorption coefficient, $h\nu$ is incident photon energy, A is the proportionality constant which is determined by index of refraction, electron and hole effective mass; however, it is usually taken as 1 for amorphous materials regardless of photon energy, E_g is the band gap energy and γ indicates the nature of electronic transition. $\gamma = 2$ indicates direct allowed transitions (direct band gap) and $\gamma = \frac{1}{2}$ indicates indirect allowed transitions (indirect band gap). $\gamma = \frac{2}{3}$ indicates the direct forbidden transitions. $\gamma = \frac{1}{3}$ indicates indirect forbidden transitions. But, the allowed transitions typically dominate the basic absorption processes, giving either direct or indirect transitions. The absorption coefficient α associated with the strong absorption region of the sample, absorbance (A) and the cuvette thickness (t) are related as below [25,26]

$$\alpha = 2.303\frac{A}{t} \quad (7)$$

Fig. 5(a) shows the absorption spectra of CaF_2 nanoparticles taken at room temperature in the range 200–700 nm using Perkin Elmer Spectrophotometer. It is observed that the characteristic absorption occurs in the UV region. For pure CaF_2 nanoparticles, the absorbance decreases exponentially with increase in wavelength and any other absorption band is not observed. This indicates the absence of any major defects like anti-Frenkel defects involving equal concentrations of negative interstitials and vacancies in the synthesized pure CaF_2 nanoparticles [27]. However, the possible defects in pure CaF_2 nanoparticles are produced by electronic excitation only and not by displacement due to momentum transfer to crystal lattice. This leads to exhibit the possible direct electronic transition so that the synthesized pure CaF_2 would become a direct band gap material. M. Khan *et al.* reported the similar absorption spectrum of CaF_2 nanoparticles having direct band gap [28]. G.W. Rubloff had also reported that CaF_2 in bulk state shows a direct band gap at the Γ point of the first Brillouin zone of 12.1 eV and an indirect band gap of 11.8 eV [29]. So the graph between $\mathbf{h\nu}$ vs $\mathbf{(\alpha h\nu)^2}$ is plotted for pure CaF_2 nanoparticles and shown

in Fig. 5(b). The intercept of the extrapolated straight line at the $(\alpha h\nu)^2 = 0$ axis gives the value of E_g of the materials. The values of E_g for pure CaF_2 nanoparticles is found to be 3.87 eV. This value is very small as compared to the value in bulk state of CaF_2 i.e. 12.1 eV. The decrease in band gap energy of pure CaF_2 when its size is reduced to nanoscale, is due to quantum confinement effect. In bulk state of CaF_2, the band gap energy is solely determined by its electronic structure as a whole. However, as the size of CaF_2 crystal decreases in nanoscale, the spatial confinement of electrons and holes increases thereby altering the electronic band structure in such a way that the energy levels become more discrete. This leads to reduction of band gap energy of pure CaF_2 nanoparticles.

Fig. 6(a) shows the absorption spectrum of CaF_2:Eu^{3+} nanoparticles taken at room temperature in the range 200–700 nm using Perkin Elmer Spectrophotometer. It is observed from figure 6(a) that the absorbance curve of Eu^{3+} doped CaF_2 i.e. CaF_2:Eu^{3+} nanoparticles consists of the absorption band at 264 nm which is attributed due to the major defects such as Schottky in CaF_2:Eu^{3+} nanoparticles [30]. Reddy and Pandurangappa also reported the spectroscopic studies in pure and Dy doped nanocrystalline CaF_2 and the similar absorption band was observed [23]. Further, during the process of electronic excitation in Eu^{3+} ion doped CaF_2 possessing schottky defect, the transfer of momentum to crystal lattice might occur through various mechanisms including interactions with lattice vibrations, charge carriers, external stimuli and relaxation processes which was also reported in literatures [31]. This leads to exhibit the possible indirect electronic transition so that the synthesized CaF_2:Eu^{3+} would become an indirect band gap material. So, the graph between $\mathbf{h\nu}$ vs $(\boldsymbol{\alpha h\nu})^{\frac{1}{2}}$ is plotted for CaF_2:Eu^{3+} nanoparticles and is shown in Fig. 6(b). The intercept of the extrapolated straight line at the $(\boldsymbol{\alpha h\nu})^{\frac{1}{2}} = 0$ axis gives the value of E_g of the materials. The value of E_g for Eu^{3+} doped CaF_2 i.e. CaF_2:Eu^{3+} nanoparticles is found to be 4.99 eV. This indicates that the band gap energy CaF_2 nanoparticles increases by 1.12 eV on doping of Eu^{3+}. The increase in band gap energy on doping of Eu^{3+} can be attributed due to the introduction of Schottky defect which is observed in absorption spectrum of CaF_2:Eu^{3+} nanoparticles as shown in Fig. 6. These defects might create localized states within band gap. This in turn leads to increase the width of band gap and hence band gap energy increases. Mele *et al.* also reported similar results on band gap and defect states in calcium fluoride [32].

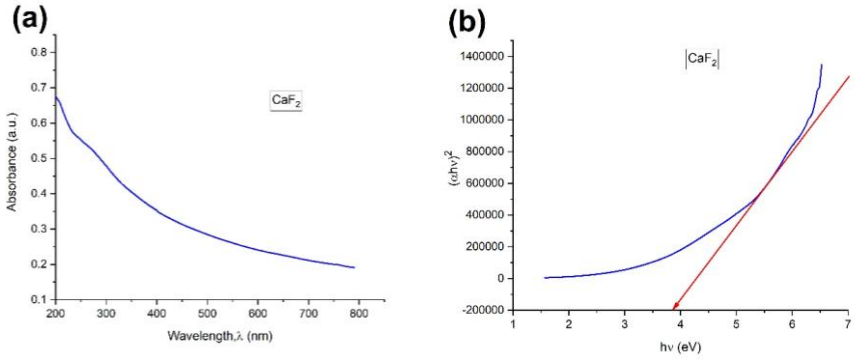

Fig. 5. (a) Absorbance Spectrum of pure CaF_2, (b) Tauc curve i.e. hν vs $(\alpha h\nu)^2$.

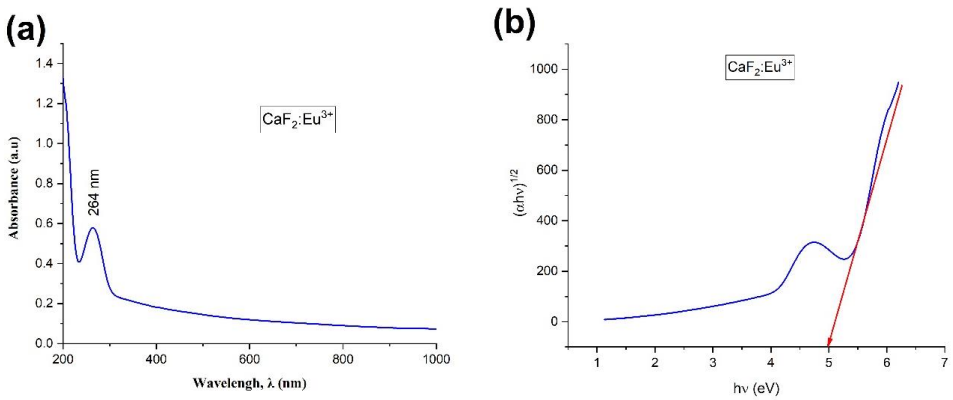

Fig. 6. (a) Absorbance spectrum of CaF_2:Eu^{3+}, (b) Tauc curve i.e. hν vs $(\alpha h\nu)^{1/2}$.

3.5. *Photoluminescence study*

Fig. 7(a) shows PL excitation spectrum of the pure CaF_2 nanoparticles. The excitation spectrum is obtained by scanning the sample at 240 nm/min at a pre-defined wavelength range, 200 – 400 nm at room temperature using Perkin Elmer Spectrophotometer. The excitation peak is observed at 387 nm which corresponds to the absorption of ultraviolet (UV) light. This reveals the optical transparency of CaF_2 in the UV range. This PL excitation might be attributed due to electronic transitions from the ground state, $^{7}\mathbf{F_0}$ to $^{5}\mathbf{G_6}$ excited state.

Fig. 7(b) shows the PL emission spectrum of pure CaF_2 nanoparticles at room temperature. The PL emission peaks is observed at 420 nm. Such type of PL emission band might be due to the formation of colour centre like F centre which is created by the presence of fluorine vacancies with an electron trapped in it, which is surrounded by four nearest neighbour calcium atoms and six second-nearest neighbour fluorine atoms. Gibin George et al. also had observed similar results in the study of size and concentration-dependent Eu^{2+}/Eu^{3+} mixed luminescent characteristics of rare-earth-doped CaF_2 nanoparticles [33]. Thus, the emission band lies in the visible region of violet colour and this property makes CaF_2 nanoparticles a potential candidate for violet lasers which can be used in dental bleaching.

Fig. 8(a) shows the PL excitation spectrum of Eu^{3+} ion doped CaF_2 i.e. CaF_2:Eu^{3+} nanoparticles at room temperature. The main excitation peaks of Eu^{3+} are observed at 317nm, 361nm and 394 nm, which might be attributed due to transition from the ground state $^{7}\mathbf{F_0}$ to excited states : $^{5}\mathbf{H_6}$ (317 nm), $^{5}\mathbf{D_4}$ (361 nm) and $^{5}\mathbf{L_6}$ (394 nm which is strongest). Furthermore, there is also a weak peak at 299 nm which would have a little effect on the excitation of Eu^{3+} [34]. Yang *et al*. also studied the luminescence properties of monodisperse spherical CaF_2 and CaF_2:Ln^{3+} (Ln = Eu, Tb, Ce/Tb) microcrystals and observed the similar results [35].

Fig. 8(b) shows the PL emission spectrum of Eu^{3+} ion doped CaF_2 i.e. CaF_2:Eu^{3+} nanoparticles at room temperature. The Eu^{3+} ion acts as a well known activator mostly showing its emission in the visible regions because this ion gets introduced into the host of CaF_2 matrix in its Eu^{3+} form. The emission peak at 591 nm corresponds to transition from excited state, $^5\mathbf{D_0}$ to low energy state, $^7\mathbf{F_1}$ and emission peak at 616 nm corresponds to transition from excited state, $^5\mathbf{D_0}$ to low energy state, $^7\mathbf{F_2}$ respectively. It is observed that the intense emission peak at 591nm confirms the incorporation of Eu ion in CaF_2 nanoparticles in the 3+ state. Further, it might be also noted that the $^5\mathbf{D_0} \rightarrow {}^7\mathbf{F_1}$ transition is allowed by magnetic dipole mechanism and the $^5\mathbf{D_0} \rightarrow {}^7\mathbf{F_2}$ transition is allowed by a hypersensitive electric dipole mechanism. Thus, the emission bands lie in the visible region of orange colour and this property makes CaF_2: Eu^{3+} nanoparticles a potential candidate for orange lasers which can be used in sodium guide star, holographic imaging and material analysis etc.

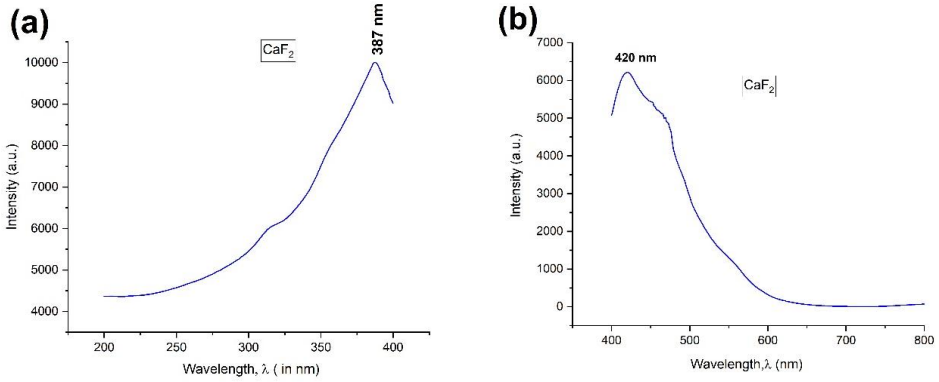

Fig. 7. (a) PL excitation spectrum of pure CaF_2, (b) PL emission spectrum of pure CaF_2.

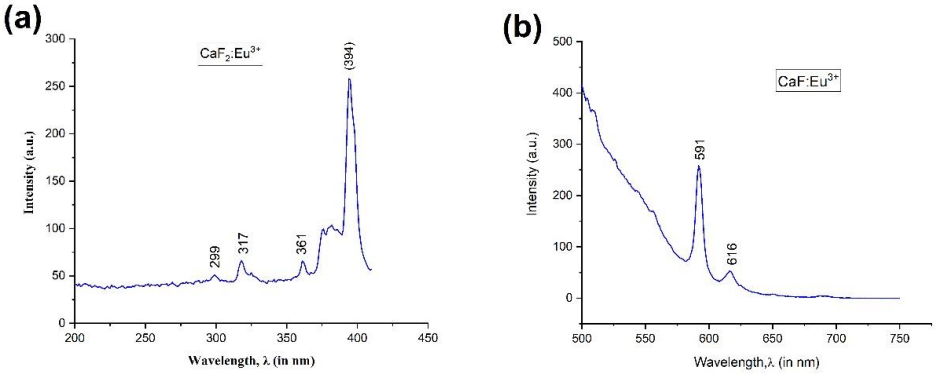

Fig. 8. (a) PL excitation spectrum of CaF_2:Eu^{3+}, (b) PL emission spectrum of CaF_2:Eu^{3+}

4. Conclusion

In summary, the pure CaF_2 and Eu^{3+} ion doped CaF_2 i.e. CaF_2:Eu^{3+} nanoparticles were synthesized successfully by following solution combustion method. The structural characterization was done by XRD and the average crystallite size for pure CaF_2 nanoparticles was found to be 17.11 nm. On doping of Eu^{3+} ion, the crystallite size increases and the average crystallite size for CaF_2:Eu^{3+} nanoparticles was found to be 32.53 nm. The elemental composition was analysed by EDAX and no impurity is present in the synthesized samples. The surface morphology was studied by FESEM and formation of nanospheroids is observed. The average diameter of nanospheroids in CaF_2:Eu^{3+} is larger than that in CaF_2. The band gap energy of the synthesized samples was estimated from UV-Visible absorption spectra. The pure CaF_2 was obtained as direct band gap material and the corresponding band gap energy is found to be 3.87 eV. However, on doping of Eu^{3+} ion, nature of band gap is transformed to indirect band gap and the corresponding band gap energy of CaF_2:Eu^{3+} was found to be 4.99 eV. From the photoluminescence study, it was observed that the emission band for pure CaF_2 nanoparticles was observed at 420 nm and it can be used as the potential candidate for fabrication of violet laser. For Eu^{3+} ion doped CaF_2 nanoparticles, the emission bands was observed at 591 nm and 616 nm respectively and it can be used as the potential candidate for fabrication of orange laser.

Acknowledgments

The authors are thankful to Nano Mission Laboratory (DST, Government of India), Thoubal College, Thoubal, Manipur for providing the facility to synthesize the sample and NIT, Manipur for providing the facilities for XRD and PL measurements of the sample, Physics Department, Manipur University, Canchipur, Manipur for measurement of UV-Visible spectroscopy and EDAX and SAIC, Institue of Advanced Study in Science and Technology (IASST), Guwahti for measurement of FESEM.

References

1. W. Ming, Z. Jiang, G. Luo, Y. Xu, W. He, Z. Xie, D. Shen, and L. Li, Nanomaterials **12**, 1491 (2022). https://doi.org/10.3390/nano12091491
2. A. d. Pablos-Martín, A. Duran, and M. J. Pascual, Int. Mater. Rev. **57**, 165 (2012).
3. J. Ding, B. Zhao, W. Ma, H. Yu, X. Qian, L. Kong, J. Wang, G. Xie, A. Wu, F. Zeng, and L. Su, Int. J. Optics **2018**, ID 8592359 (2018). https://doi.org/10.1155/2018/8592359
4. S. Fujihara, Y. Kadota, T. Kimura, J. Sol-Gel Sci. Technol. **24**, 147 (2002). https://doi.org/10.1023/A:1015252010509
5. Z. Fang, H. Yu, B. Zhang, D. Jiang, Q. Wu, L. Xiong, H. Zhao, and L. Su, J. Lumin. **233**, ID 117877 (2021). https://doi.org/10.1016/j.jlumin.2020.117877
6. E. Cantelar, J. A. Sanz-García, A._a. Sanz-Martín, J. E. M. Santiuste, and F. Cusso, J. Alloys Compds. **813**, ID 152194 (2020). https://doi.org/10.1016/j.jallcom.2019.152194
7. D. Malviya, V. B. Pawade, and B. A. Bhanvase, Luminescence **34**, 426 (2019). https://doi.org/10.1002/bio.3630
8. A. Bensalah, M. Mortier, G. Patriarche, P. Gredin, and D. Vivien, J. Solid State Chem. **179**, 2636 (2006). https://doi.org/10.1016/j.jssc.2006.05.011

9. B. C. Hong and K. Kawano, Japanese J. Appl. Phys. **46**, 6319 (2007). https://doi.org/10.1143/JJAP.46.6319
10. L. Song and L. Xue, Appl. Surf. Sci. **258**, 3497 (2012). https://doi.org/10.1016/j.apsusc.2011.11.102
11. G. Wang, Q. Peng, and Y. Li, J. Am. Chem. Soc. **131**, 14200 (2009). https://doi.org/10.1021/ja906732y
12. G. L. Zhi, J. H. Song, B. C. Mei, and W. B. Zhou, J. Alloy Compds. **509**, 9133 (2011). https://doi.org/10.1016/j.jallcom.2011.06.084
13. D. S. Zheleznov, A. V. Starobor, and O. V. Palashov, Optical Mater. **46**, 526 (2015). https://doi.org/10.1016/j.optmat.2015.05.018
14. S. Anghel, S. Golbert, A. Meijerink, and A. -V. Mudring, J. Lumin. **189**, 2 (2017). https://doi.org/10.1016/j.jlumin.2016.10.007
15. F. Wang and X. G. Liu, Chem. Soc. Rev. **38**, 976 (2009). https: //doi.org/10.1039/B809132N
16. L. Wang, B. Wang, W. X. Wang, J. Liu, Tribol. Int. **40**, 1179 (2007). https://doi.org/10.1016/j.triboint.2006.12.003
17. C. Pandurangappaa, B. N. Lakshminarasappa, B. M. Nagabhushana, J. Alloy Compds. **489**, 592 (2010). https://doi.org/10.1016/j.jallcom.2009.09.118
18. X. Sun and Y. Li, J. Chem Commun. 1768 (2003). https://doi.org/10.1039/B303614F
19. O. Roth, H. Hasselberg, and M. Jonsson, J. Nucl. Mater. **383**, 231 (1009). https://doi.org/10.1016/j.jnucmat.2008.09.026
20. A. Taylor, X-ray Metallography (John Wiley & Sons, Inc., New York, 1961).
21. J. Pan, K. Zhong, Z. Zhang, W. Chen, Y. Lin, G. Wang, L. Li, and Y. Yui, Optical Mater. Express **8**, ID 2782 (2018). https://doi.org/10.1364/OME.8.002782
22. B. C. Hong and K. Kawano, J. Alloy Compds. **451**, 276 (2006). https://doi.org/10.1016/j.jallcom.2007.04.056
23. G. N. V. Reddy and C. Pandurangappa, Int. J. Mech. Eng. **7**, 1 (2022).
24. Amorphous and Liquid Semiconductor, ed. J. Tauc (Plenum Press, New York, 1974).
25. A. Cottrell, Introduction to Mettallurgy (Arnold, London, 1975).
26. R. S. Longhurst, Geometrical and Physical Optics (Longman Group Limited, U.K., 1957).
27. R.W. Ure, J. Chem. Phys. **26**, 1363 (1957). https://doi.org/10.1063/1.1743547
28. M. E. Khan, F. Alam, A. Parveen, and A. H. Naqvi, Structural, J. Adv. Microscopy Res. **8**, 45 (2013). https://doi.org/10.1166/jamr.2013.1135
29. G. W. Rubloff, Phys. Rev. B **5**, 662 (1972). https://doi.org/10.1103/PhysRevB.5.662
30. S. Kulshrestha, S. Khan, S. Hasan, M. E. Khan, L. Misba, and A. U. Khan, Appl. Microbiol. Biotechnol. **100**, 1901 (2016). https://doi.org/10.1007/s00253-015-7154-4
31. J. C. Krupa and A. Meijerink, J. Phys.: Cond. Matter **12**, 3531 (2000).
32. E. J. Mele, S. W. Kirchoefer, and T. F. Deutsch, Phys. Rev. B (1986).
33. G. George, J. I. Hayes, C. N. Collins, J. E. Davis, L. Yu, Y. Lin, J. Wen, D. Ila, Z. Luo, J. Alloy Compds. **857**, ID 157591 (2021). https://doi.org/10.1016/j.jallcom.2020.157591
34. L. G. DeShazer, G. H. Dieke, J. Chem. Phys. **38**, 2190 (1963). https://doi.org/10.1063/1.1733949
35. X. Yang, J. Cao, and S. Hu, Int. J. Mater. Sci. Applicat. **5**, 54 (2016).